Characterization of Deep Geothermal Energy Resources in Low enthalpy sedimentary basins in Belgium using Electro-Magnetic Methods – CSEM and MT results

Nicolas Coppo, Mathieu Darnet, Virginie Harcouet-Menou, Pierre Wawrzyniak, Adele Manzella, François Bretaudeau, G. Romano, D. Lagrou, Jean-Francois Girard

Characterization of Deep Geothermal Energy Resources in Low enthalpy sedimentary basins in Belgium using Electro-Magnetic Methods – CSEM and MT results

Coppo N. [1], Darnet M.[1], Harcouët-Menou V. [2], Wawrzyniak, P. [1], Manzella A. [3], Bretaudeau F. [1], Romano G. [4], Lagrou D. [2] and Girard J.-F. [5]

[1] B.R.G.M., 3 avenue Claude-Guillemin, BP 36009 - 45060 Orléans cedex 2 – France

[2] VITO, Boeretang 200, BE-2400 Mol, Belgium.

[3] CNR, Instituto di Geoscienze e Georisorse, 1 Via Giuseppe Moruzzi, 56124 Pisa – Italy

[4] University of Bari, Dipartimento di Scienze della Terra e Geoambientali, 4 Via Orabona, 70121 Bari – Italy

[4] Prior at B.R.G.M., now at IPGS, 5 rue René Descartes, Strasbourg, France

Corresponding author: n.coppo@brgm.fr

Keywords: Geothermal exploration, Electro-Magnetic Methods, Magneto-Telluric, Controlled-Source Electro-Magnetic, MT, CSEM, Low enthalpy Geothermal Reservoir.

ABSTRACT

Sedimentary basins in Northwest Europe have significant potential for low to medium enthalpy, deep geothermal energy resources. These resources are generally assessed using standard seismic exploration techniques to resolve geological structures. The Electro-Magnetic campaign carried-out in Mol area (Belgium) has shown that despite the presence of high level of industrialization, the resistivity of deep formations (>3km) can be recovered from MT and CSEM methods and hence provide very valuable information for the assessment of geothermal resources.

1. INTRODUCTION

Sedimentary basins in Northwest Europe have significant potential for low to medium enthalpy, deep geothermal energy resources. These resources are generally assessed using standard seismic exploration techniques to resolve geological structures. However, the electrical resistivity parameter, which can be directly impacted by the presence of a geothermal reservoir is rarely investigated in such context. Therefore, the development of alternative and complementary exploration techniques such as Electromagnetic (EM) techniques may have an important role in reducing the cost and uncertainty associated with geothermal resource assessment.

While EM techniques have proven to be useful in geothermal exploration in high enthalpy areas in the last decades only a handful of studies assessed their applicability in low enthalpy sedimentary basins (Bujakowski et al., 2010). There, challenges include identifying which sub-surface features cause changes in electrical resistivity as low enthalpy reservoirs are unlikely to exhibit the hydrothermally altered clay layer above the geothermal aquifer that is typical for high enthalpy reservoirs. Yet a principal challenge is likely to be the high level of industrialization in the areas of interest. Infrastructure such as train tracks and power cables can create a high level of background noise that can obfuscate the relevant signal.

In September 2015, VITO (Flemish Institute for Technological Research) started drilling an exploration well for a deep geothermal project at the Balmatt site in Mol (Belgium). The first well was successfully completed in January 2016, reaching the Carboniferous Limestone Group at a depth of 3175 m. Formation temperature at a depth of 3600 m reached 138°C and production tests confirmed the geothermal potential of the limestones. In this context, an EM campaign was conducted in July 2015 near the Balmatt site in Mol. Using electo-magnetic measurements to investigate the deep geothermal potential in Belgium, which is densely populated and highly industrialized, was as such, a real challenge. The possibility of using classical magnetotelluric (MT) passive technique to aid identification of geothermal resources has been tested. In addition, to overcome the problem of high level of noise expected in the region and generally crippling for MT data, CSEM (controlled source EM) measurements have been performed and lead to reliable results.

2. CSEM/MT SURVEY LAYOUT

Pre-survey 3D CSEM modelling (POLYEM, Bretaudeau et al., 2015) was used to test different source configurations and select a reasonable transmitter-receiver offset. According to the survey duration and objectives, a WSW-ENE 18 km-long

profile of 9 MT/CS stations has been selected to be acquired (Figure 1). The (a-priori) resistivity model (13 layers) was based on resistivity logs available in surroundings boreholes. A 2-D conductive anomaly was incorporated in the geometry of the Lower-Carboniferous limestones (target layer) at the depth of about ~3000 m. These results indicated that the conductive anomaly could be detected for periods longer than 8 seconds using surface-surface injection dipole at about 6 km from the profile, i.e. in near field configuration for the frequencies of interest. In far field conditions, results showed that resolving the expected conductive anomaly could be difficult.

Therefore, according to local constrains we installed a double orthogonal dipole surface-surface (L-shape) of 2 x 1 km north of the profile providing the two first polarizations (Figure 1, POL1 and POL2). The closest and farthest stations (CS5 and CS0) were located at about 6 and 12 km respectively. We then moved to a third polarization (POL3) using two 600-m boreholes as long electrodes for current injection (see Bourgeois et al. (2010) for details). In this paper, we will focus mainly on the results of polarizations 1 and 2, and on the MT data.

The 9 MT/CSEM stations were all deployed in the field during the first week of July 2015 (Figure 1). We used seven Metronix (four ADU06 and three ADU07) and two Zen Zonge full MT stations with both MFS06 and MFS07 magnetic sensors with non-polarizable Pb-Cl electrodes. Ten to fifteen 1 m-long metallic sticks were used on each pole for current injection with salty water (POL1 and POL2). Current injection was performed with the TXM22 transmitter of Metronix during the day. Magnetotelluric data were collected during the night to take advantage of the higher signal to noise ratio. A remote reference was set up at the Geophysical Center at Dourbes (Belgium) for further robust data processing. A surficial sandy layer prevented an ideal current injection and limited it to about 18-20 A (up to 128Hz) for polarization 1 and 2. On polarization 3, we reached 40-45A using energized casings. A set of frequencies ranging from 32 s to 512 Hz by multiple of 2 has been acquired on all polarizations. Higher frequencies up to 8192 Hz have been collected on stations (CS1, CS2 and CS3) due to sampling frequency limitations and logistics. Up to 720 periods were collected at the 32 s transmitted period and more for higher frequencies.

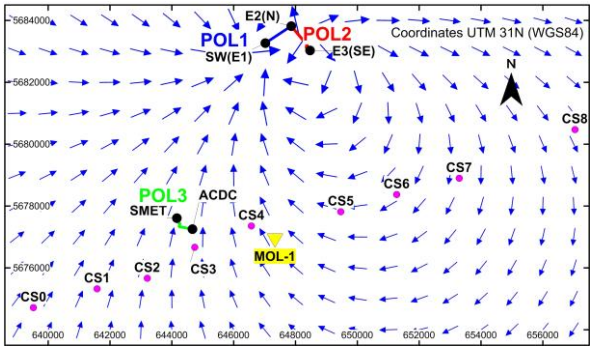

Figure 1: CSEM/MT survey layout. CS0 to CS8 MT/CS stations. Location of the 3 dipoles (polarizations) used for current injection with electric field (in-phase) distribution at frequency 0.125 Hz in a 50 Ωm homogeneous medium drawn for POL1 only. The location of the new deep geothermal exploration well MOL-1 is represented by the yellow triangle.

3. CSEM/MT PROCESSING

3.1 CSEM Data Processing

Data have been processed using BRGM proprietary software. Transfer function between the recorded signals (electric and magnetic fields) and the transmitted electric current are estimated in the Fourier domain for each fundamental frequency and harmonics. The obtained complex transfer functions represent the electric and magnetic earth response to a unitary current injection.

A high level of cultural noise is expected in the area of interest due to the proximity of the industrial activities. A typical example of noise is shown on Figure 2 where we can observe a well pronounced peak of energy at 50Hz and its harmonics caused by power lines. Given the diversity and intensity of EM noises present in the dataset, we used both frequency domain noise level estimates as well as manual inspection of the amplitude spectra to accept or reject the electric fields recorded at all stations and frequencies of interest. Out of the nine CSEM stations, two turned out to be too noisy to be useful. This demonstrates that in such an environment and despite using an active source, a great care must be taken in planning the survey in order to select recording sites with sufficient signal to noise ratios.

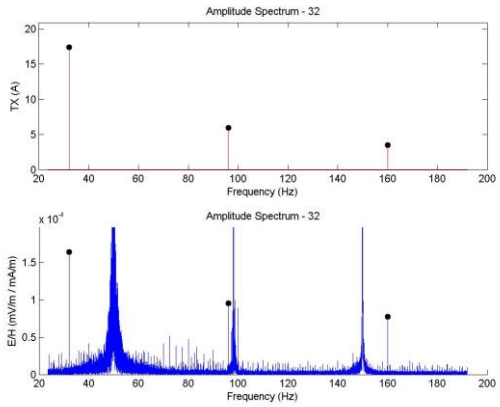

Figure 2: Top: amplitude spectrum of the transmitted current. Bottom: amplitude spectrum of the recorded electric field. Please note the high level of anthropic noise (50Hz and harmonics), stronger than the recorded electric field at the CSEM frequency.

3.2 MT Data Processing and Quality Check

Data from sites 0 to 8 were processed using BRGM own robust processing code (Razorback, developed by Smai and Wawrzyniak at the BRGM). Remote reference bounded influence processing (Chave et al., 2004) was performed between synchronous measurements on the profile and improved data quality by filtering incoherent noise. Due to low signal to noise ratio, sites 6 and 8 were excluded. MT soundings (i.e apparent phase and resistivty curves) from sites 0 to 5 and 7 only were kept in the interpretation.

After this first QC, consistency checks have been performed on the obtained MT soundings. Sites 0 and 3 were subsequently excluded. We also observed a polarized noise on the NS component of the electric field, which reduces the quality of xy components, especially at low frequency for sites 2 and 4, while the yx components are more coherent. Consequently, biased frequency bands of the MT soundings were also discarded, such as component xy for site 2 and 4. Remaining MT soundings are sites 1 (xy and yx) , 2 (yx), 4 (yx), 5 (xy and yx), 7 (xy and yx) as showed on Figure 3. After complete QC, only site 7 shows a reliable MT sounding on both xy and yx components over the frequency band of interest (0.01Hz<f<1Hz).

Looking at ρ^a_{yx} on the high frequency band (500Hz-1kHz), all sites converge to an approximate median value of ρ^a_{yx} of 80 Ω.m. Then, ρ^a_{yx} decreases with frequency to a median minimum value of 10 Ω.m between 0.5Hz and 5 Hz. For frequencies under 0.5Hz, ρ^a_{yx} increases up to 40-50 Ω.m for sites 1 and 5 while sites 2, 4 and 7 reach only 20 Ω.m.

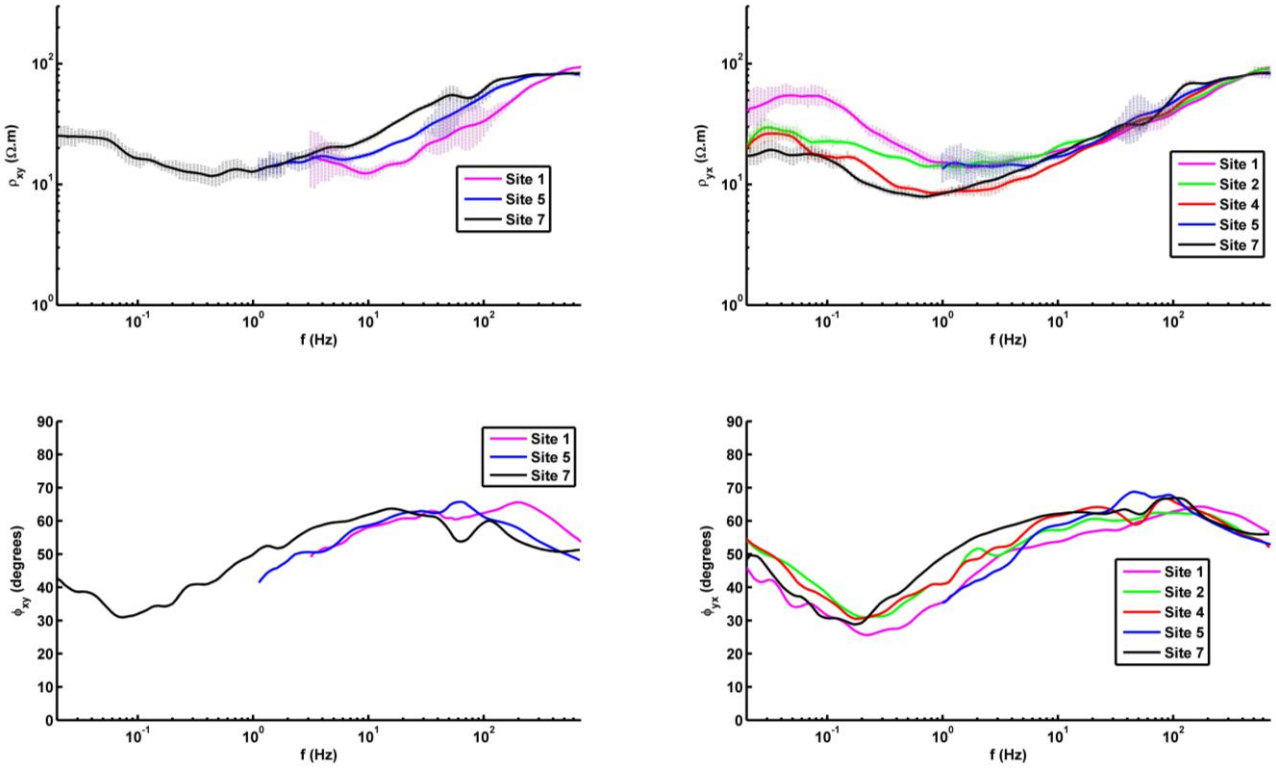

Figure 3: Remaining MT soundings apparent resistivity (upper pannel) and phase (lower pannel) for sites 1,2, 4, 5 and 7. Left panel, top : apparent resistivity xy (Ω.m), bottom : apparent phase xy (degrees). Right panel, top : apparent resistivity yx (Ω.m), bottom : apparent phase yx (degrees). Error bars are shown on the resistivity curves as vertical dashed lines.

4. 1D CSEM/MT INVERSION

4.1 OCCAM1D Inversion

To derive resistivity vs depth profiles from the CSEM or MT data, we used the smooth 1D inversion code designed by Constable et al. (1987) and Key (2009) called OCCAM1D. In a nutshell, it seeks to minimize the following unconstrained regularized functional:

$$U = \|\partial \mathbf{m}\|^2 + \|\mathbf{P}(\mathbf{m} - \mathbf{m}_*)\|^2 + \mu^{-1}\left[\|\mathbf{W}(\mathbf{d} - F(\mathbf{m}))\|^2 - \chi_*^2\right] \quad [1]$$

The first term is a norm of the model roughness and is computed by applying a differencing operator ∂ to the elements of the model vector **m**. For the one dimensional models considered here, m is a vector of $\log_{10}\rho$ for each layer and ∂ is chosen to be a matrix of first-differencing operators so that ∂m approximates the vertical derivative of $\log_{10}\rho$. The second term is a measure of the difference of **m** from an a priori preference model **m***. The diagonal matrix P contains scaling parameters that determine the relative weighting between the preference and the model roughness. The roughness and preference terms in the above equation are regularizers that serve to stabilize the inversion and keep it from producing wildly oscillating resistivity structure. Finally, the third term is a measure of the misfit of the model's forward response **F(m)** (i.e., the electric and magnetic fields for model **m**) to the data **d**. **W** is a data covariance weighting function and is here selected to be a diagonal matrix with elements corresponding to inverse data standard errors. In other words, **W** weights the relative contribution of each datum to the misfit based on its uncertainty. χ_*^2 is the target misfit and its inclusion illustrates that minimizing ***U*** does not necessarily find the best fitting model, but rather a smooth model that is within the specified target misfit (usually chosen to be unity). The Lagrange multiplier $\boldsymbol{\mu}$ serves to balance the trade-off between the data fit and the model roughness and model preference. The nonlinear minimization of equation is described in Constable et al. (1987) and one of the main innovations of the Occam method is the automatic selection of $\boldsymbol{\mu}$.

4.2 CSEM Results

Figure 4 shows the 1-D inversion resistivity profile (in red) obtained from the smooth inversion of the CSEM data transmitted at 0.03125, 0.0625, 0.125, 0.25, 4, 8, 16, 32, 64, 128, 256, 512 Hz and both polarizations (POL 1 and POL2) and recorded at stations 00, 01, 02, 03, 06 and 07. For comparison, the resistivities logged in the nearby geothermal exploration are also displayed (in blue). The fit between the modelled and observed data is good (standard deviation of misfits of less than 10%), demonstrating that the inversion has converged. We only inverted the maximum axis of the polarization ellipses of the electric field, as the minor components sometimes turned out to be too noisy.

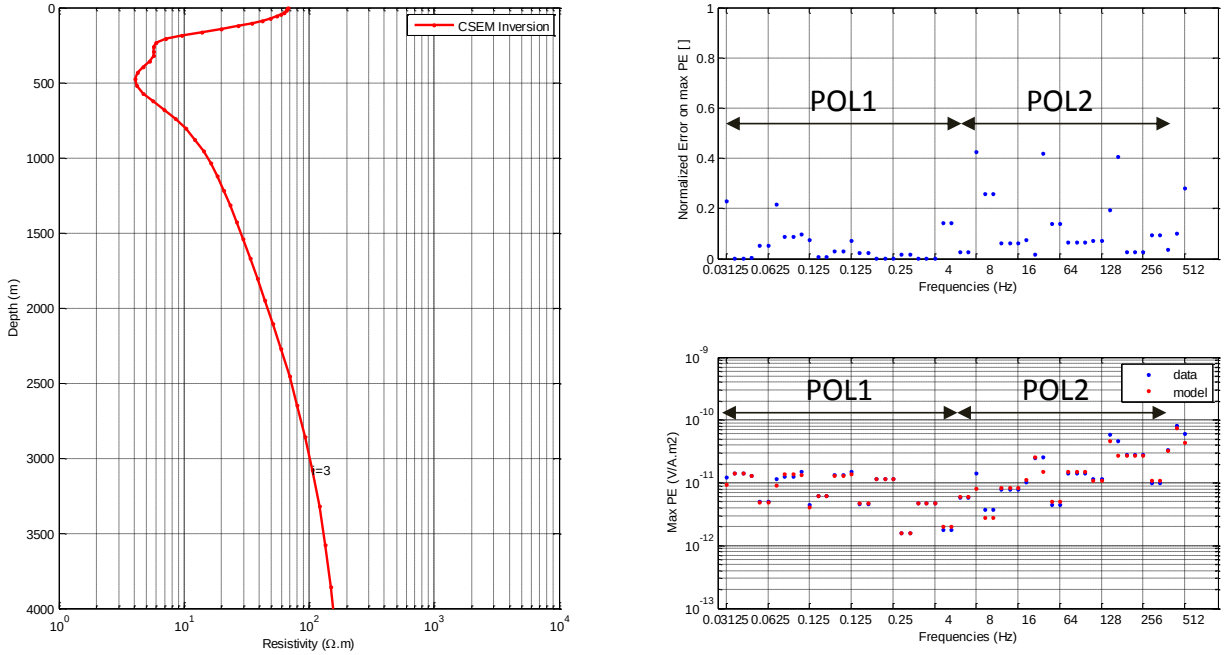

Figure 4: Left: 1-D inversion (red) resistivity profile obtained from the smooth inversion of the CSEM data transmitted at 0.03125, 0.0625, 0.125, 0.25, 4, 8, 16, 32, 64, 128, 256, 512 Hz and both polarizations and recorded at stations 00, 01, 02, 03, 06 and 07. Top right: relative misfit between the modelled and observed CSEM data. Bottom right: observed (blue) versus modelled (red) maximum axis of the polarization ellipse of the horizontal electric field.

4.3 MT results

Because of cultural noise contamination, only the apparent resistivities and phases of the YX impedance

tensor have been inverted. Figure 5 shows the resistivity profile derived from the inversion of the MT data from the site 04, in the middle of the CSEM array and next to the geothermal exploration well. The overall misfits between modelled and observed data (right panels on Figure 5) are very good (less than 10% in the frequency band of interest, 0.05Hz to 500Hz).

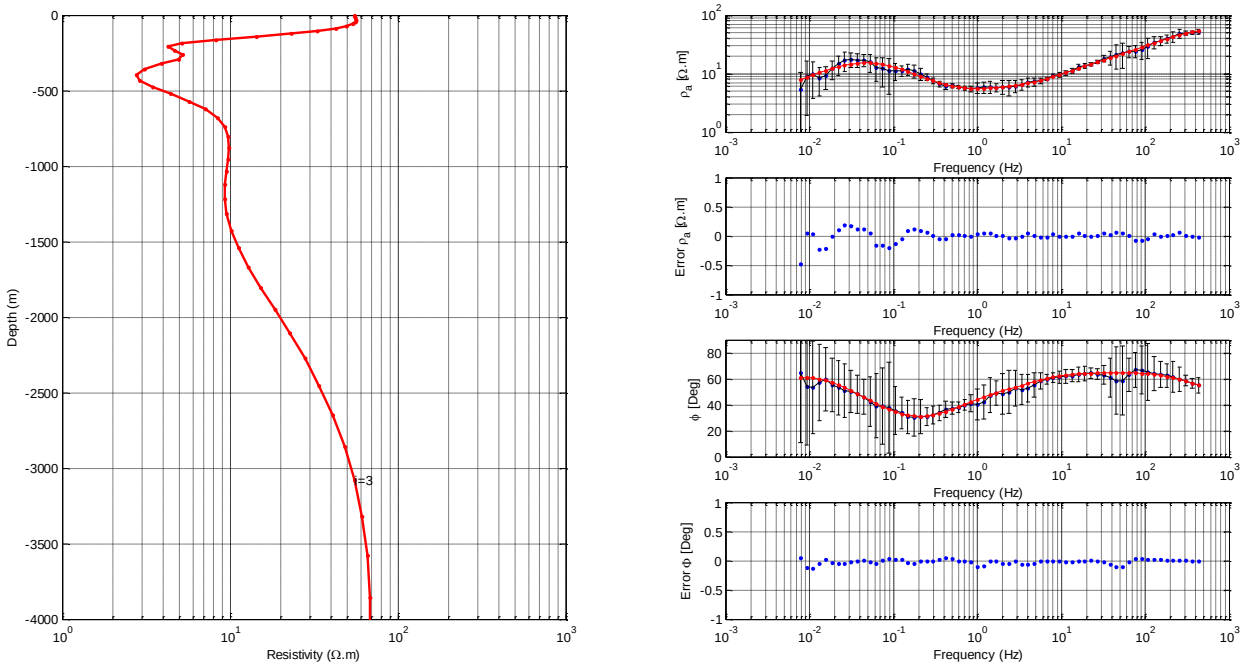

Figure 5: Left: 1-D inversion (red) resistivity profile obtained from the smooth inversion of the MT data between 0.01 and 1000Hz at stations 04. Top right: observed (blue on top subplot) versus modelled (red on top subplot) apparent resistivities and relative misfit (bottom subplot) between the modelled and observed apparent resistivities of the Zyx impedance tensor. Top right: observed (blue on top subplot) versus modelled (red on top subplot) phases and relative misfit (bottom subplot) between the modelled and observed phases of the Zyx impedance tensor.

4.3 Discussion

The 1D resistivity profile obtained from the inversion of the MT and CSEM data (Figure 6) fits the logged values at the nearby geothermal exploration very well in the shallow section (<1500m) and reasonably well in the deeper section (1500 – 3500m depth). The shallow resistive body (depth < 200m, ρ≈50 Ω.m) corresponds to recent (Quaternary and Neogene) sediments (sands, gravels). Underneath, more conductive (ρ<10 Ω.m) Paleogene and Cretaceaous sediments (claystones, siltstones, sandstones and chalk) can be found up to 900 m depth. At that depth, older sediments are encountered (Carboniferous claystone/sandstone with coal and finally Lower-Carboniferous limestones) and resistivities steadily increase again (15 Ω.m in the Cretaceous limestones, 20 Ω.m in the Carboniferous claystone/sandstone with coal and 100 Ω.m in the Lower-Carboniferous limestones).

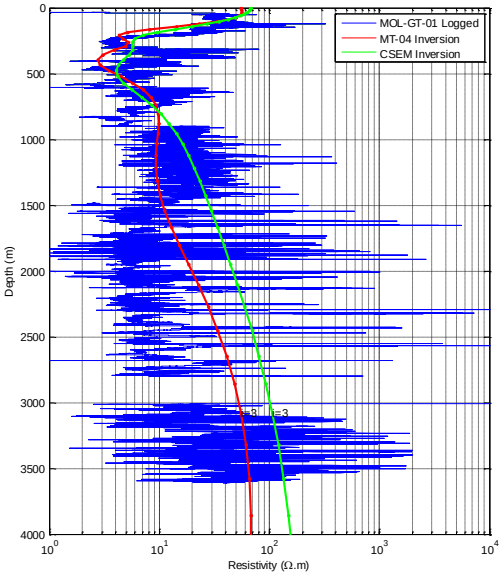

Figure 6: Resistivity profile obtained from the smooth inversion of the CSEM (green) and MT (red) data. For comparison, the

resistivities logged with deep induction tools in the nearby geothermal exploration are also displayed (blue).

To validate the inversion results in the deeper section, we inverted synthetic CSEM data generated at the same sites and frequencies as the actual CSEM survey on a resistivity model derived from the geothermal exploration well (Figure 7). 10% Gaussian noise has been added to the maximum of the polarization ellipses to simulate actual data. Here also, the inversion has converged well with residuals of less than 10% (Top right on Figure 7).

Due to the diffusive nature of the EM waves at these frequencies, the inverted resistivity profile captures well the average resistivity of the different units but not precisely the actual depth of the different interfaces. To improve even further the inversion result, additional constraints would have to be provided in the form of a priori information (e.g. depth of interfaces from seismic data). A similar behavior can be observed on the inversion results of the actual CSEM and MT data (Figure 6). This demonstrates that the resistivities from the CSEM and MT inversions are actually matching the logged resistivity values very well, both in the shallow and deep sections. We however observe that CSEM resistivities in the older sediments are larger than the MT resistivities by roughly a factor two. We believe this discrepancy is caused by the sequence of thin conductive (e.g. shales) and resistive (e.g. coal) layers, as evidenced by the well logs, that creates macroscopic electrical anisotropy (Brown et al., 2010). The MT soundings are more likely to be sensitive to the horizontal resistivity while the CSEM soundings are more likely to be sensitive to the vertical one.

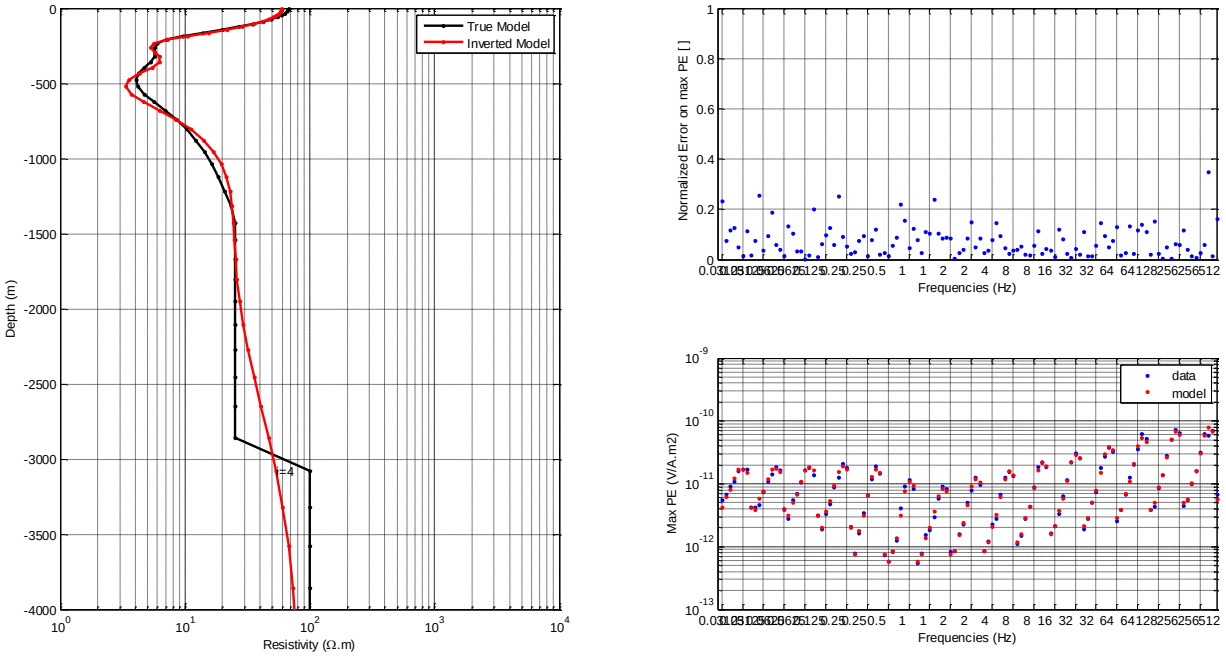

Figure 7: Left: 1-D inversion (red) resistivity profile obtained from the smooth inversion of synthetic CSEM data generated at 0.03125, 0.0625, 0.125, 0.25, 4, 8, 16, 32, 64, 128, 256, 512 Hz and simulated at stations 00 to 08. For comparison, the true resistivity profile is also displayed (black). Top right: relative misfit between the modelled and observed CSEM data. Bottom right: observed (blue) versus modelled (red) maximum axis of the polarization ellipse of the horizontal electric field.

The target geothermal reservoir lies in the potentially fractured Lower Carboniferous Limestone Group. The resistivity log shows that when the exploration well penetrates the interval comprising fissured limestones, the logged resistivity abruptly dropped from 100 Ω.m to less than 10 Ω.m (locally down to 1 Ω.m. To further characterize the geothermal potential of the area of interest, we therefore propose to use resistivity measurements as a proxy for the degree of fracturation/alteration and presence of geothermal fluid. It is therefore important to establish whether accurate resistivities of the target formation can actually be derived from the CSEM data. To do so, we tested the sensitivity of a CSEM station 10 km away from the source to a drop of resistivity from 100 Ω.m to 10 Ω.m of the target limestones (Figure 8). It creates a CSEM anomaly of around 50% of the total horizontal electric field, i.e. well above the noise level observed during the CSEM survey (around 10%). This demonstrates that the CSEM method is capable of sensing the resistivity drop of the limestone caused by the presence of a large-scale network of dissolution enlarged fissures and therefore potentially identify the areas favourable for the development of a geothermal system.

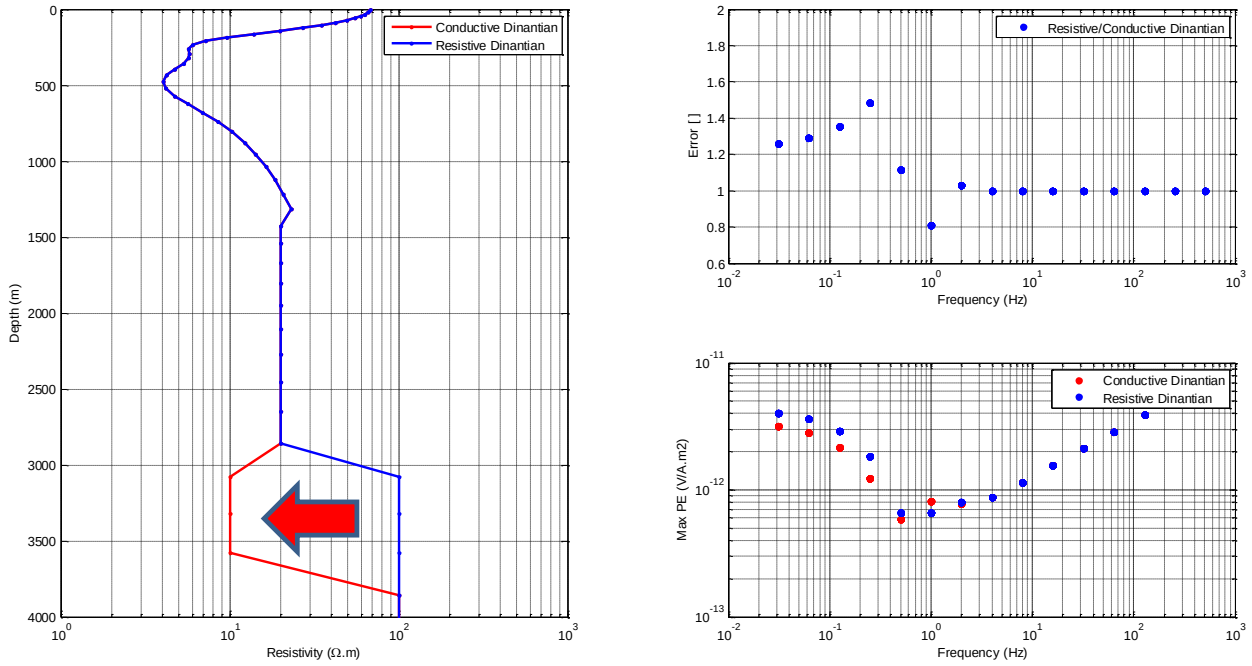

Figure 8: Left: Resistivity model for a fissured (red) and intact (blue) limestone reservoir. Right: amplitude (bottom) and relative change (top) of the maximum axis of the polarization ellipse of the horizontal electric field 10km way from the CSEM source as a function of the CSEM source frequency.

3. CONCLUSIONS

Sedimentary basins in Northwest Europe have significant potential for low to medium enthalpy, deep geothermal energy resources. These resources are generally assessed using standard seismic exploration techniques to resolve geological structures. The Electro-Magnetic campaign carried-out in Mol (Belgium) has shown that despite the presence of the high level of industrialization, the resistivity of deep formations (>3km) can be recovered from MT and CSEM methods and hence provide very valuable information for the assessment of geothermal resources. We therefore believe Electromagnetic (EM) techniques are complementary exploration techniques that will have an important role to play in reducing the cost and uncertainty associated with geothermal resource assessment.

ACKNOWLEDGEMENTS

Mr Rasson and prof. Hus of the Geophysical Center at Dourbes are tanked for their cooperation to install the remote reference. The landowners are thanked to let us install the measuring equipment on their property. VITO would like to thank former colleague Sian Loveless who initiated the research project.

This research receives support of the European Union, the European Regional Development Fund ERDF, Flanders Innovation & Entrepreneurship and the Province of Limbug.

REFERENCES

Bourgeois B. and Girard J. F. (2010) – First modelling results of the EM response of a CO2 storage in the Paris Basin. Oil & Gas Science and Technology– Revue de l'Institut Français du Pétrole, 65(4), 597-614.

Bretaudeau F., Wawrzyniak P., Coppo N. and Girard J.-F. (2015) – Reconstruction 3-D de la résistivité électrique par méthode inverse en CSEM avec 1 unique émetteur. Proceedings of Journée de l'AGAP Qualité, Grenoble, 2015.

Brown V., M. Hoversten, K. Key, and J. Chen (2011) – Resolution of reservoir scale electrical anisotropy from marine CSEM data. Geophysics, vol. 77 (2), E147–E158, doi: 10.1190/GEO2011-0159.1.

Bujakowski W, Barbacki A, Czerwińska B, Pająk L, Pussak M, Stefaniuk M, Trześniowski Z. (2010) – Integrated seismic and magnetotelluric exploration of the Skierniewice, Poland, geothermal test site. Geothermics, 39 (1), 78–93, doi: 10.1016/j.geothermics.2010.01.003.

Bujakowski W. (2010) – The use of geothermal waters in Poland (state in 2009). Prz Geol. 58 (7), 580-588.

Chave AD, Thomson DJ (2004) – Bounded influence magnetotelluric response function estimation. Geophys. J. Intern, 157 (3), 988-1006.

Constable, S. C., R. L. Parker, and C. G. Constable, (1987) – Occam's inversion – A practical algorithm for generating smooth models from electromagnetic sounding data. Geophysics, 52, 289–300.

Kerry K. (2009) – 1D inversion of multicomponent, multifrequency marine CSEM data: Methodology and synthetic studies for resolving thin resistive layers, Geophysics, 74 (2), F9–F20, doi: 10.1190/1.3058434.